

Article pubs.acs.org/accounts

Reaction Mechanisms, Kinetics, and Improved Catalysts for Ammonia Synthesis from Hierarchical High Throughput Catalyst Design

Jon Fuller, Qi An,* Alessandro Fortunelli,* and William A. Goddard, III*



ACCESS

Cite This: Acc. Chem. Res. 2022, 55, 1124-1134

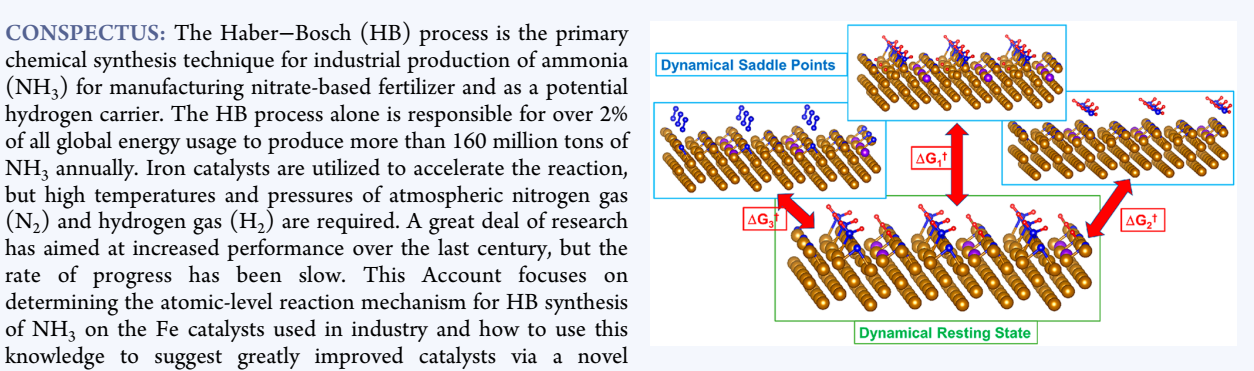
paradigm of catalyst rational design.



Article Recommendations

CONSPECTUS: The Haber-Bosch (HB) process is the primary chemical synthesis technique for industrial production of ammonia (NH₃) for manufacturing nitrate-based fertilizer and as a potential hydrogen carrier. The HB process alone is responsible for over 2% of all global energy usage to produce more than 160 million tons of NH₃ annually. Iron catalysts are utilized to accelerate the reaction, but high temperatures and pressures of atmospheric nitrogen gas (N₂) and hydrogen gas (H₂) are required. A great deal of research has aimed at increased performance over the last century, but the rate of progress has been slow. This Account focuses on determining the atomic-level reaction mechanism for HB synthesis of NH3 on the Fe catalysts used in industry and how to use this

Metrics & More



Supporting Information

We determined the full reaction mechanism on the two most active surfaces for the HB process, Fe(111) and Fe(211)R. We used density functional theory (DFT) to predict the free-energy barriers for all 12 important reactions and the 34 most important 2 × 2 surface configurations. Then we incorporated the mechanism into kinetic Monte Carlo (kMC) simulations run for several hours of real time to predict turnover frequencies (TOFs). The predicted TOFs are within experimental error, indicating that the predicted barriers are within 0.04 eV of experiment.

With this level of accuracy, we are poised to use DFT to improve the catalyst. Rather than forming bulk alloys with uniform concentration, we aimed at finding additives that strongly prefer near-surface sites so that minor amounts of the additive might lead to dramatic improvements. However, even for a single additive, the combinations of surface species and reactions multiplies significantly, with \sim 48 reaction steps to examine and nearly 100 surface configurations per 2 \times 2 site. To make it practical to examine tens of dopant candidates, we developed the hierarchical high-throughput catalysis screening (HHTCS) approach, which we applied to both the Fe(111) and Fe(211) surfaces. For HHTCS, we identified the most important 4 reaction steps out of 12 for the two surfaces to examine >50 dopant cases, where we required performance at each step no worse than for pure Fe. With HHTCS, the computational cost is about 1% of that for doing the full reaction mechanism, allowing us to do ≈50 cases in about 1/2 the time it took to do pure Fe(111). The new leads identified with HHTCS are then validated with full mechanistic studies.

For Fe(111), we predict three high-performance dopants that strongly prefer the second layer: Co with a rate 8 times higher, Ni with a rate 16 times higher, and Si with a rate 43 times higher, at 400 °C and 20 atm. We also found four dopants that strongly prefer the top layer and improve performance: Pt or Rh 3 times faster and Pd or Cu 2 times faster. For Fe(211), the best dopant was found to be second-layer Co with a rate 3 times faster than that for the undoped surface.

The DFT/kMC data were used to predict reshaping of the catalyst particles under reaction conditions and how to tune dopant content so as to maximize catalytic area and thus activity. Finally, we show how to validate our mechanistic modeling via a comparison between theoretical and experimental operando spectroscopic signatures.

■ KEY REFERENCES

• Qian, J.; An, Q.; Fortunelli, A.; Nielsen, R. J.; Goddard, W. A. Reaction Mechanism and Kinetics for Ammonia Synthesis on the Fe(111) Surface. J. Am. Chem. Soc. 2018, 140, 6288-6297. This work reports the NH₃ reaction mechanism we determined on the Fe-bcc(111) surface.

Received: December 20, 2021 Published: April 7, 2022





- Fuller, J.; Fortunelli, A.; Goddard, W. A.; An, Q. Reaction Mechanism and Kinetics for Ammonia Synthesis on the Fe(211) Reconstructed Surface Phys. Chem. Chem. Phys. 2019, 21, 11444–11454.² This work reports the NH₃ reaction mechanism on the Fe-bcc(211)R surface as well as the favorable reconstruction for Fe-bcc(211) under reaction conditions.
- An, Q.; Shen, Y.; Fortunelli, A.; Goddard, W. A. QM-Mechanism-Based Hierarchical High-Throughput in Silico Screening Catalyst Design for Ammonia Synthesis. J. Am. Chem. Soc. 2018, 140, 17702–17710.³ This work develops and demonstrates the HHTCS approach to the discovery of promising dopants to enhance catalytic reaction rates.
- An, Q.; Mcdonald, M.; Fortunelli, A.; Goddard, W. A. Si-Doped Fe Catalyst for Ammonia Synthesis at Dramatically Decreased Pressures and Temperatures. J. Am. Chem. Soc. 2020, 142, 8223–8232. This work details our discovery via HHTCS of the best single-dopant on Fe-bcc surfaces.

1. INTRODUCTION

The development of much more highly active and selective industrial catalysts with minimal waste and environmental impact is extremely important, but it is most challenging to make dramatic improvements. Much of the progress to date has been driven by empirical trial and error with serendipity often playing a role. But the challenges in energy and environment demand much faster progress with clear guidelines on the most promising directions. To go beyond trial-and-error approaches, we must provide a basis to rational catalyst design, through a foundational understanding of the target reaction mechanisms combined with efficient high-throughput protocols. We have initiated investigations along these lines, which we review herein, using the Haber-Bosch (HB) ammonia (NH₃) synthesis using Fe-based catalysts⁵ as a paradigmatic example to illustrate and demonstrate our theoretical/computational approach and its possible synergy with experimental validation and realization. The complexity of the reaction mechanisms for N₂ reduction to NH₃, with multiple potentially rate-determining reaction steps, and their interplay with the catalyst structure and composition, the presence of dopants and promoters, as well as the effect of the support make HB ammonia synthesis a realistic prototypical industrial catalytic process, where dozens of reaction steps combine to make the ideal catalyst a unique species, at the intersection of numerous Brønsted-Evans-Polanyi (BEP) energy relationships in a fragmented descriptor landscape.

The synthesis of NH₃ using the HB process, first performed industrially in the 1910s, is one of the most critical synthesis processes in the world today. Many industries rely on the HB process, especially nitrate-based fertilizer production consuming over 160 million tons of NH₃ every year. The HB process involves reacting nitrogen gas (N₂) from the atmosphere with hydrogen gas (H₂) extracted primarily by water gas shift (CO + H₂O \rightarrow H₂ + CO₂) in high-pressure (200 atm) high-temperature reactors facilitated with an iron-based catalyst. Current iron-based catalysts are reliable and cost-effective, typically achieving efficiencies of up to 70% under standard industrial conditions. However, efficient synthesis of NH₃ requires the reaction to be performed under high temperatures typically in the range of 700–800 K coupled with pressures in the range of 50–200 atm. Sustaining these high temperatures

and pressures in a controlled environment requires a tremendous amount of energy; thus, the HB process currently accounts for over 2% of global energy consumption.8 Research into improved catalyst design to achieve less-intensive conditions has been conducted for decades, but success has been slow and incremental. On the fundamental side, a significant amount of information has been accumulated. Reaction rates and mechanisms have been investigated through several experimental techniques starting from the 1980's pioneering work by Ertl.9 and followed by comprehensive studies by Somorjai and co-workers. 10-13 Somorjai and Materer examined the active low index surfaces involved in NH3 synthesis, finding that Fe-bcc(111) and Fe-bcc(211) were significantly active with a 100:75 relative ratio, 11 while other surfaces, such as Fe-bcc(100) and Fe-bcc(110), were roughly an order of magnitude less active. Specifically, they found a TOF of 9.7 NH₃ molecule/sec/site on Fe-bcc(111) under the conditions: T = 673 K and P = 15/5/0.002 atm for H₂, N₂, and NH₃, respectively. They also suggested that 4-fold binding sites on the surfaces aid NH3 formation by successive hydrogenation and explained the discrepancy in activity due to the prevalence of such sites on the closely packed Fe-bcc(111) and Fe-bcc(211) surfaces and their relative absence on the others (see Figure S1 in the Supporting Information for an atomistic view of the involved facets and the 4-fold-or C7binding sites as discussed in the original experimental work). 12,13 The role of promoters was also quantified, with K promotion increasing the TOF on catalytically active Fe-bcc surfaces by a factor $\approx 2.^{10}$ Importantly, the rate of NH₃ synthesis on the single-crystal Fe-bcc(111) and Fe-bcc(211) surfaces is roughly similar to the reported rates for the commercial Fe catalyst with a 94% Fe composition and 5.9% promoter oxides with an observed TOF of $\approx 0.1-1$ NH₃ molecule/s/active site at T = 673 K, $P = 7.5/2.5 \text{ atm for H}_2 \text{ and N}_2$, respectively, under flow conditions. 14 This indicates that single crystals are relevant systems for assessing catalyst efficiency for direct comparison to industrial systems. Also important, neutron diffraction experiments on industrial Fe catalysts have indicated that the bulk of the industrial catalyst exhibits a bcc crystal structure, implying that calculations on slabs exposing extended facets should provide realistic models of this system. 15 In the experimental work, the influence of reaction conditions on catalytic activity was finally assessed, finding a strong "ammonia poisoning" effect, i.e., a strong reduction of catalytic rates when increasing ammonia pressure. This was associated with cases in which ammonia adsorbs on empty sites of the catalyst in competition with the N2 molecule, thus preventing N2 from absorbing and becoming activated. 10 There were also experimental indications of a similar "hydrogen poisoning" effect. Thus, H₂ molecules can adsorb dissociatively to "poison" catalytically active empty sites. Coverage ("poisoning") effects on catalysis will be discussed extensively in the discussion below. More subtle coverage phenomena have also been pointed out. For example, the adsorption energy of an adsorbate on a catalyst depends strongly on the coverage of various surface species, 16 the N binding energy changes significantly with the coverage of surface species for $\mathrm{NH_3}$ synthesis on Ru catalyst, 17 and the surface coverage of K species can change the electronic environment of various Fe crystal planes. 18 More recently, computational techniques have been used to investigate binding sites, transition states, and other mechanistic information on NH3 synthesis on several surface orientations of bcc Fe^{1,2,19} and other systems such as metal nitrides.²⁰ In particular, the adsorption behavior of the intermediate species important for NH₃ synthesis and how binding sites influence transition states in the synthesis reaction has been an important area of computational research. Additionally, computational screening techniques have been applied to both rutile oxides²² and transition metals²³ for electrochemical catalyst designs proposed for NH₃ synthesis. However, relatively little computational screening has been applied to the Fe catalytic surfaces prior to our works. ^{3,4,19,21}

Alternatives to HB synthesis have been proposed but have not yet matched industrial requirements for high-efficiency and economical large-scale production of NH₃.²⁴⁻²⁸ Ru-based catalysts exhibit a higher efficiency compared to the current Fe based catalysts, but industry has been reluctant to adopt them due to higher cost and environmental concerns.²⁴ Electrochemical techniques that supply H from water rather than from gas-phase H₂ have the advantages of eliminating the huge CO₂ production of the water gas shift reaction while operating under drastically lower temperatures and pressures, but sustainability of electrochemical reduction has not been demonstrated at the industrial scale.²⁵ Intensively investigated "green" NH₃ synthesis using renewable energy such as solar-powered photocatalysis for NH₃ photofixation requires semiconductor photocatalysts combined with advanced material design, usually involving either expensive or toxic metals, while not yet producing NH3 at industrial-scale levels. 26,28 These techniques remain relatively premature for use in industrial applications.

Herein, we summarize our recently proposed theoretical framework for designing improved catalysts for mechanistically complex, industrially relevant reactions, as schematically illustrated in Figure 1, which we exemplify for HB NH₃

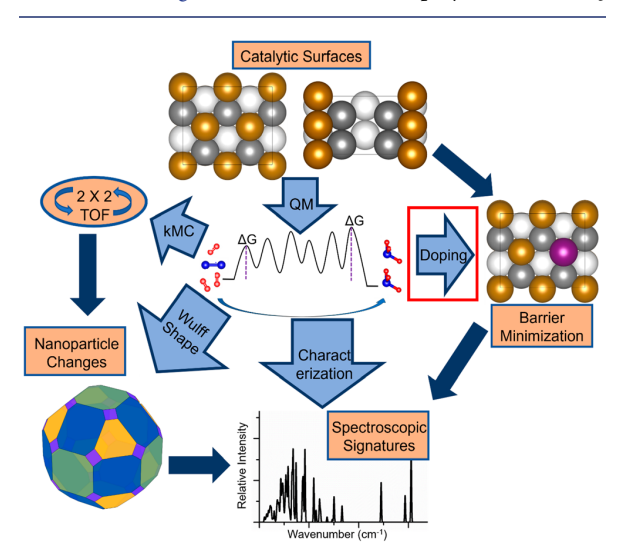


Figure 1. Overview of our theoretical framework for catalyst design.

synthesis on Fe-bcc doped single-crystal surfaces. First, we combine quantum mechanics (QM) and kinetics modeling to determine the detailed reaction mechanism (12 independent reaction steps for HB) and reaction rates on the two key surface orientations, Fe-bcc(111)¹ and Fe-bcc(211)R.² Then, we describe how to enhance catalytic efficiency via surface selective doping using hierarchical high-throughput catalyst screening (HHTCS).³ HHTCS enables us to optimize binary catalysts undergoing the same basic reaction mechanism, but with much reduced overall reaction barriers, to produce much higher

reaction rates. This should translate into lowering operating temperatures and pressures to provide improved energy usage at constant throughput.⁴ Next, we extend the HHTCS approach by including the surface energy of Fe nanoparticles to predict nanoparticle reshaping and how this can be exploited to maximize the catalytically active surface area.²⁹ Finally, we discuss how to translate this accumulated information into predicting spectroscopic features that can be used to monitor the catalysis and validate the reaction mechanism using in situ/operando or ex situ techniques.³⁰

2. THE HABER-BOSCH REACTION MECHANISM ON Fe SURFACES

2.1. Fe-bcc(111) NH₃ Synthesis Reaction Mechanism

The Fe-bcc(111) surface is one of the two key surface orientations for efficient NH $_3$ synthesis. ¹¹ Fe-bcc(111) prevails in NH $_3$ synthesis by a 100:75 ratio ¹¹ compared to the second most efficient surface, Fe-bcc(211), with a turnover frequency (TOF) = 9.7 NH $_3$ molecules/s per 2 × 2 site at temperature T = 673 K and pressures P = 15/5/0.002 atm for H $_2$, N $_2$, and NH $_3$, respectively, compared to TOF = 7.3 NH $_3$ molecules/second per 2 × 2 site on Fe-bcc(211) at undisclosed low NH $_3$ pressure. We focused first on determining the reaction mechanism on the Fe-bcc(111) surface using QM. We used a six-layer Fe slab model with the bottom three layers fixed and the top three layers allowed to relax. We performed density functional theory (DFT) calculations, ³¹⁻³³ employing the Perdew–Burke–Ernzerhoff (PBE) ^{34,35} functional with D3 empirical corrections for dispersive interactions (PBE-D3). ³⁶ Transition states were determined using the Nudged Elastic Band (NEB) approach. ³⁷

The computational model is shown in Figure 2. We find that

- H atoms prefer 2-fold bridging sites in between first/ second or first/third layer surface Fe atoms
- N atoms prefer the 2-fold bridge site between two firstlayer Fe atoms, while
- NH_x species prefer a succession of sites from 2-fold bridge sites for N and NH to first/second-layer bridge site for NH₂, and then finally a top site bound solely to a first-layer Fe atom for NH₃, prior to desorption from the surface.¹

These results are in good agreement with previous work. The bridge sites are most important for catalysis, with four in a (2 × 2) cell; thus, the adsorbate configuration with all four occupied by N adatoms is labeled as 4N and similarly for the other configurations (see ref 1 for a more precise nomenclature). The reaction mechanism involves a Langmuir—Hinshelwood (LH) mechanism with successive hydrogenation (that is, the formation of NH_x species sequentially on the surface from successive addition of H) via H surface migration. The Eley–Rideal (ER) hydrogenation mechanism (hydrogenation directly from gas phase, without surface migration) was found to be energetically preferable only in a minority of cases, such as the initial hydrogenation from the 4N configuration to 3N-NH-H. The overall reaction free-energy diagram (FEdiag) and mechanism are shown in Figure 3.

In agreement with previous theoretical analysis, $^{1,19,21}_{,1}$ breaking the strong N_2 triple bond requires two neighboring empty bridge sites on the surface. This leads to a multistep mechanism:

- N₂ binds first in a σ-mode (retaining a N≡N triple bond) perpendicular to the surface on a top-layer Fe atom,
- then it overcomes a barrier to adsorb on a second-layer Fe,

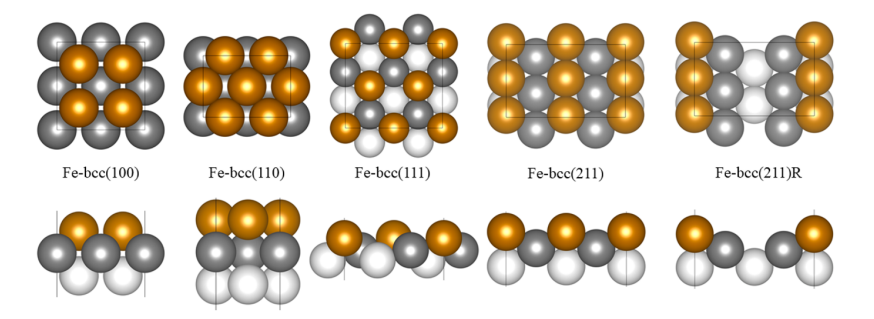


Figure 2. Surface structures of bcc Fe studied computationally for Haber–Bosch NH_3 synthesis. Bronze spheres represent first (top)-layer Fe atoms, silver spheres represent second-layer Fe atoms, and white spheres represent third-layer Fe atoms in the slab model. Top (upper row) and side (bottom row) views illustrate the differences in surface orientations. The lowest three layers of the six-layer slabs are not shown.

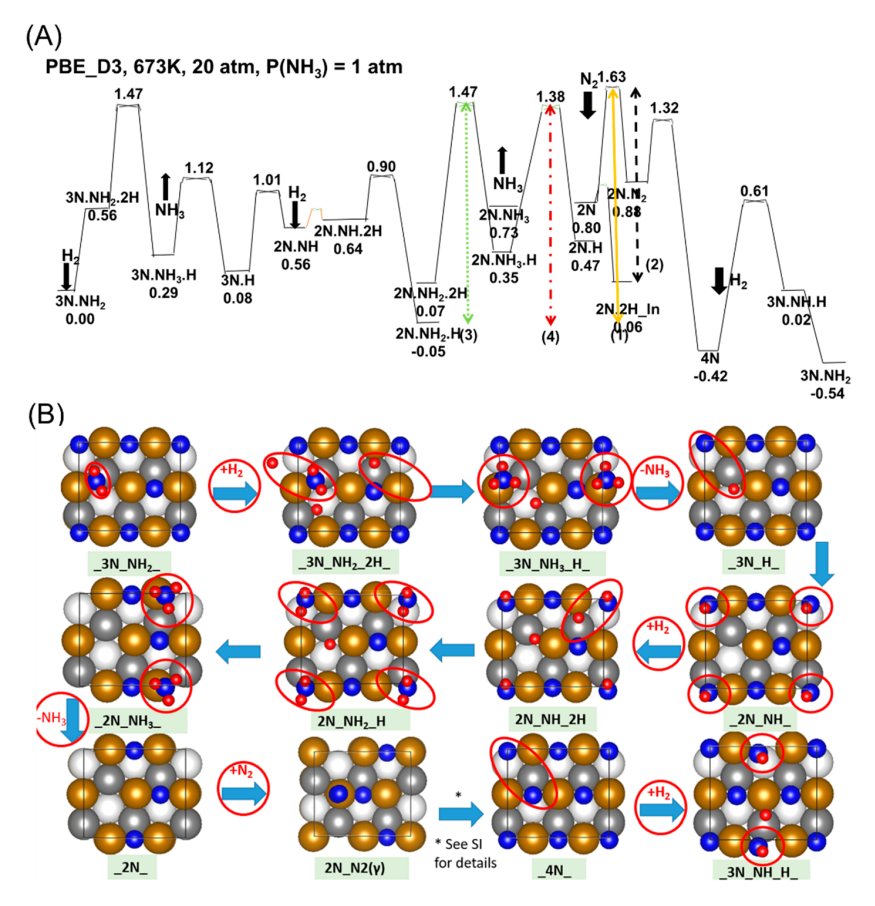


Figure 3. Quantum mechanics derived free energy diagram for Fe-bcc(111) NH₃ synthesis (A) and surface structures of key configurations for NH₃ synthesis on Fe-bcc(111) (B) at T = 673 K and $P(H_2, N_2, NH_3) = (15, 5, 1)$ atm. Color coding as in Figure 2, with N as blue spheres and H as red spheres. Red circles highlight reacting adsorbate species. The asterisk symbol (*) indicates a complex N₂ dissociation pathway (see the Supporting Information of ref 1). Energies are in eV. Panel (A) is reproduced from ref 3. Copyright 2021 American Chemical Society. Panel (B) is reproduced from ref 1. Copyright 2018 American Chemical Society.

- then it moves to a π-bond mode (with a N=N double bond) in a horizontal position across two second-layer Fe (and on top of a third-layer Fe atom),
- then it forms 2 more bonds to the surface, leaving a N-N single bond
- then it dissociates into two separate N-bridge positions.

The saddle point for N_2 dissociation is not the highest in the FEdiag on Fe-bcc(111), because at high temperatures (\geq 400

°C) it is exceeded by the N₂ adsorption barrier with its large entropic terms. The overall barrier calculated with respect to the 2N.NH₂.H dynamical resting state is equally composed of:

- the N_2 adsorption barrier (\approx 0.8 eV) to form the π -bonded state and
- the difference between the 2N.NH₂.H and 2N states (≈0.8 eV), from the free-energy cost for creating 2 neighboring empty bridge sites on the surface.

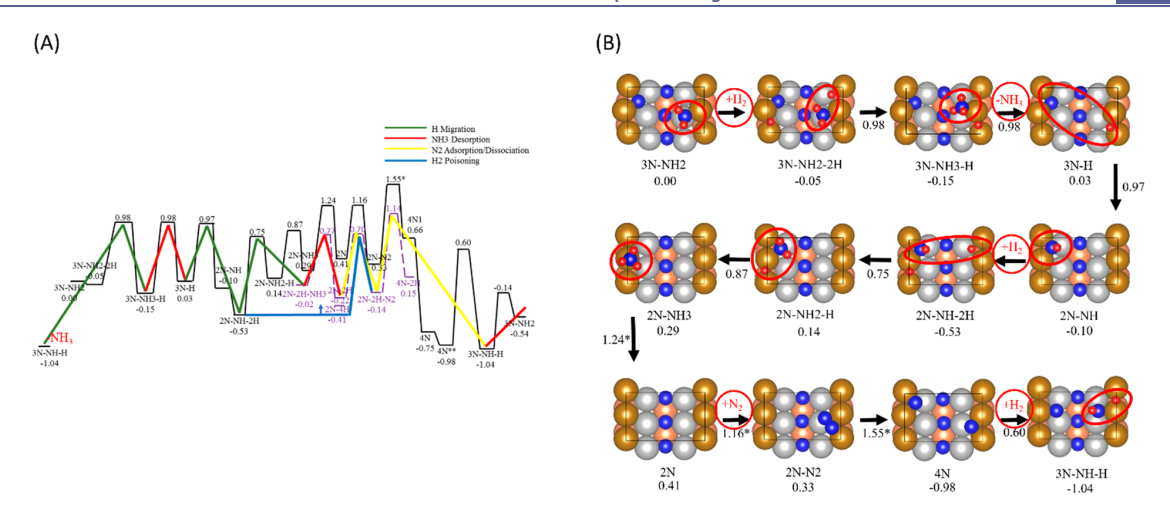


Figure 4. Quantum mechanics derived free energy diagram for NH₃ synthesis on Fe-bcc(211)R with chemically different reaction steps highlighted in color (left) and surface structures for key states in the NH₃ synthesis on Fe-bcc(211)R (right) at conditions of T = 673 K, $P(H_2, N_2, NH_3) = (15, 5, 1)$ atm. Color coding as in Figure 3. Red circles highlight reacting adsorbate species. The asterisk symbol * indicates a complex N₂ dissociation pathway (see the Supporting Information of ref 2). Energies are in eV. Panels (A) and (B) are reproduced with permission from ref 2. Copyright 2019 Royal Society of Chemistry.

The primary reaction barriers on Fe-bcc(111) are therefore

- N₂ adsorption/desorption,
- N₂ dissociation,
- hydrogenation of NH2 to form NH3, and
- NH₃ desorption from the surface.

By using the QM data in a kinetic Monte Carlo (kMC) model under Somorjai conditions (T = 673 K, P = 20 atm, $P(\text{NH}_3) = 1.5 \text{ Torr}$), we predicted a TOF = 17.7 NH₃/s per 2 × 2 site in excellent agreement with experimental TOF = 9.7 NH₃/s per site. Increasing the dominant energy barrier by 0.04 eV would lead to the experimental TOF, or it could be that only half the surface sites are active experimentally.

2.2. Fe-bcc(211)R Reaction Mechanism

We next turned our attention to the Fe-bcc(211) surface, which is the second most active experimental surface orientation. First, our calculated surface energies at T > 673 K in the presence of adsorbed N/H atoms predict that Fe-bcc(211) undergoes a missing-row reconstruction to Fe-bcc(211)R under reaction conditions, which is especially favored at the high temperatures and pressures realized in a HB reactor. 41,42 The missing-row reconstruction is catalytically relevant as it exposes additional 4fold binding sites important for NH3 synthesis (as illustrated in Figure S1). The site preference of adsorbed species on both reconstructed and unreconstructed (211) surface 43 were similar to Fe-bcc(111). Also similar to Fe-bcc(111), the N_2 dissociation pathway was found to be complex with a perpendicular to parallel tilt shift from top to second layer Fe atoms followed by dissociation into 4-fold bottom sites. The calculated full reaction path is shown in Figure 4A (the complex N₂ dissociation pathway can be found in the Supporting Information of ref.²), with the full free-energy diagram (FEdiag) in Figure 4B. The FEdiag was inputted into a kMC model to determine reaction rates using the QM free energy reaction barriers. This leads to TOF = 18.7 NH₃/s per 2 × 2 site at T = 673 K and P = 15/5/0.002 atm for $H_2/N_2/NH_3$, respectively, and TOF = 3.5 NH_3/s per 2 \times 2 site at T = 673 K and P = 15/5/1 atm on for Febcc(111). After accounting for the difference in surface area between the bcc(111) and bcc(211)R facets, this places the

relative TOF of the two surfaces in the ratio 100:99, in excellent agreement with the experimental rate ratio of 100:75. Interestingly, the kMC analysis indicates that Fe-bcc(211)R is twice more active than Fe-bcc(111) at high-pressures of P = 40/5/1 atm for $H_2/N_2/NH_3$, respectively.²

3. HIERARCHICAL HIGH-THROUGHPUT CATALYST SCREENING (HHTCS)

3.1. Kinetics Analysis

To estimate reaction rates using the QM-predicted free energy reaction barriers and the mechanisms deduced for Fe-bcc(111) and Fe-bcc(211)R we used a self-consistent kMC algorithm. The kMC approach is based on a stochastic evaluation of the reaction kinetics and is an effective method for determining resting states and lifetimes of intermediate states. Here we used a model with 100 replicas. Kinetic constants on the QM-determined reaction path were calculated via transition state theory (TST) rate = $(k_{\rm B}T/h)\exp(-\Delta G^{\dagger}/k_{\rm B}T)$, where ΔG^{\dagger} is the difference in free-energy between the initial and the transition state (saddle point) for each reaction step and $k_{\rm B}$ is the Boltzmann constant (gas-phase adsorption was modeled via the reverse desorption combined with the microscopic reversibility principle).

Essential for catalyst rational design, we then developed a simplified kinetic model. In this model, the overall catalytic reaction rate was approximated as = $(k_{\rm B}T/h)\exp(-\Delta G^\dagger/k_{\rm B}T)$, with ΔG^\dagger being the free-energy difference between the lowest-free-energy state in the FEdiag (the dynamical resting state) and the highest saddle-point (the dynamical transition state). Extensive tests showed that this simplified model approximated with extremely good precision our full kMC predicted rates. Only when the largest and the second largest barrier were very close, was a two-barrier correction formula necessary to obtain quantitative accuracy. 45

The simplified kinetic model led us to analyze the FEdiag to single out the potentially rate-limiting reaction steps in the shortest (minimum-barrier) Dijkstra path. In practice, the following reaction steps were singled out as potentially rate-

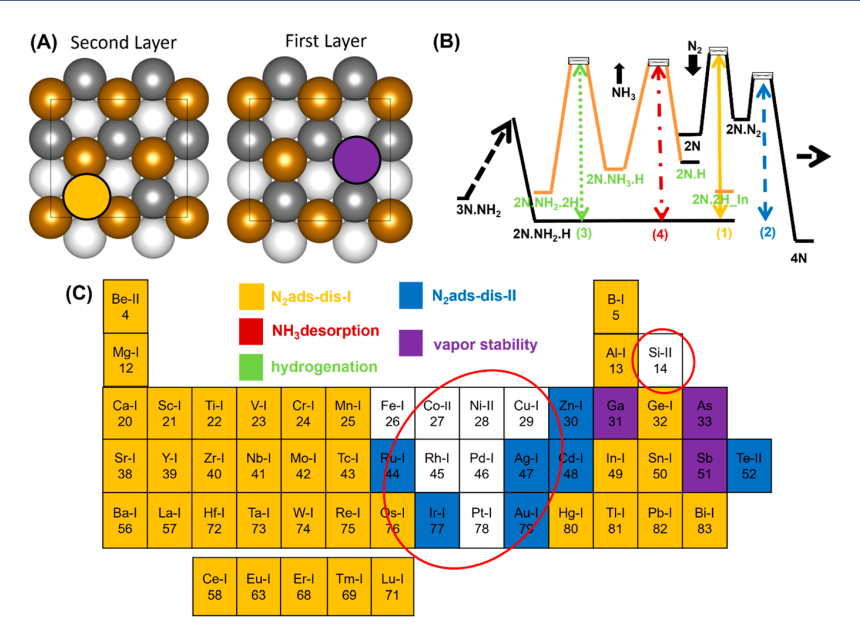


Figure 5. Application of HHTCS to Fe bcc (111). (A) First layer (purple) and second layer (yellow) doping sites on the Fe-bcc(111) surface. (B) Free-energy landscape illustrating the reaction barriers evaluated in HHTCS as colored lines: (1) in orange the primary reaction barrier, N_2 adsorption vs the $2N.NH_2$.H configuration; (2) in blue N_2 adsorption vs the 2N.2H configuration; (3) in green hydrogenation of NH_2 to NH_3 ; (4) in red NH_3 desorption. (C) Diagram showing the results of the HHTCS screening sequence: candidates eliminated due to the vapor stability criterion are represented in purple, while those eliminated by the corresponding barriers shown in (B) are shaded in the same colors as in (B). Circles highlight the best dopant candidates. Panel (B) is reproduced from ref 4. Copyright 2020 American Chemical Society.

limiting on both Fe-bcc(111) and Fe-bcc(211)R in the FEdiag of Figures 3 and 4:

- N_2 adsorption/desorption and dissociation (i.e., the $2N + N_2 \rightarrow 2N.N_2 \rightarrow 4N$ steps),
- hydrogen poisoning to the N_2 activation (i.e., the ΔG of the $2N.2H \rightarrow 2N.N_2$ process)
- hydrogenation of NH_x states, in particular, the $NH_2 \rightarrow NH_3$ step, and
- NH₃ desorption from the surface.

These rate-limiting reaction steps, highlighted in color in Figures 3 and 4, were then arranged in *hierarchical order* (decreasing barrier). We then combined QM and kinetic analysis to deploy a strategy for catalyst rational design, as described in the next section.

Note that a change in pressure or temperature may change the dynamical resting state and/or the transition state, so that the barrier ordering *depends upon reaction conditions*. One such effect is connected with hydrogen pressure and the associated H₂ poisoning phenomenon. kMC reaction rates depend upon H₂ pressure, especially for Fe-bcc(211)R for which the reaction rate can be doubled by increasing the H2 pressure from the stoichiometric condition $(P(H_2) = 15 \text{ atm})$ to $P(H_2) = 40$ atm. Similar reasoning holds for NH_3 poisoning. These observations can be rationalized in terms of the simplified kinetic model, and are in full agreement with empirical observations of poisoning effects in HB catalysis as recalled in the introduction.^{2,3,45} In brief, adsorption of a reactant or product species on empty sites of the catalyst occurs in competition with the N₂ molecule, thus preventing N₂ from absorbing and dissociating. Thus, the energy price to make catalytically active sites vacant and keep them available for reactions must be included in the overall free-energy barrier,

effectively slowing down the catalytic process, i.e., catalyst poisoning.

3.2. HHTCS Design

The HHTCS approach is a protocol for designing improved catalysts for complex-mechanism catalytic reactions such as HB NH₃ synthesis.³ Different from volcano modeling, ⁴⁶ this approach is based on the full QM-based reaction mechanism, on a simplified kinetic modeling, and on a fast but accurate prediction of the effect of a change in the catalyst structure on reaction rates. HHTCS accelerates the search over many potential doping candidates by quickly evaluating their effect on key states in the reaction pathway, whence their expected effect on a set of hierarchically ordered reaction free-energy barriers. HHTCS includes the following steps:

- (a) analyze the free-energy diagram to single-out potentially rate-determining barriers and arrange them in a hierarchical sequence;
- (b) define simple criteria to estimate the effect of a given modification in the catalyst on each barrier;
- (c) after defining a set of candidate catalyst modifications, evaluate each criterion in order of decreasing barrier, with each step restricted to candidates that passed the higherlevel screening by leading to a decreased barrier;
- (d) test the stability of proposed catalyst modification with respect to possible degradation mechanisms; and
- (e) for the best candidates that survive all previous criteria, reconstruct a free-energy diagram and perform explicit kMC simulations to accurately predict reaction rates.

The practical application to Fe-bcc(111) and (211)R in the next sections will illustrate the HHTCS protocol.

3.2.1. HHTCS: Application to Fe-bcc(111). We considered doping of 51 elements in both the first (topmost) or second

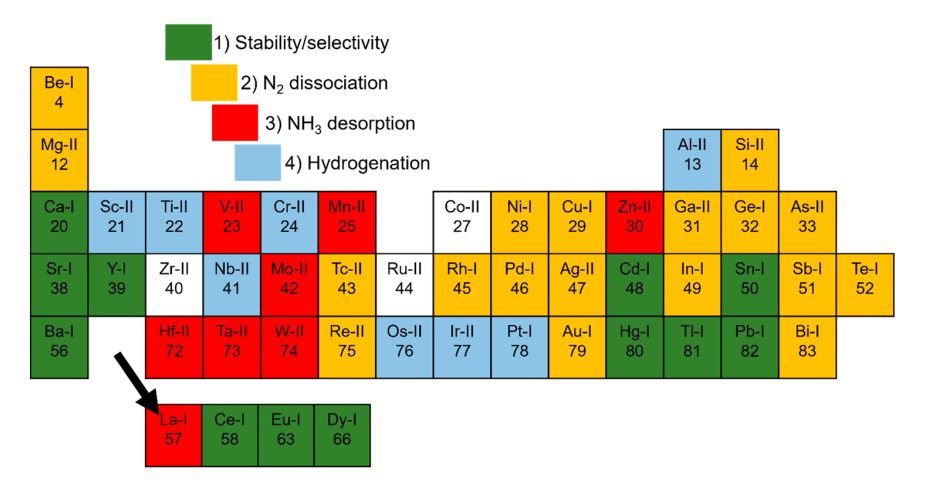


Figure 6. Application of HHTCS to Fe-bcc(211)R. The 49 elements chosen for HHTCS analysis. Radioactive as well as extremely rare or valuable metals were excluded for consideration as viable dopants. Screening results for each element are shown by shading for each criterion; stability/selectivity indicates prohibitive behavior in either layer tested that would inhibit the determined reaction mechanism. Reproduced from ref 48. Copyright 2020 American Chemical Society.

(subsurface) layers of Fe-bcc(111) as illustrated in Figure 5A. Four primary, potentially rate-determining processes influence reaction rates on Fe-bcc(111):

- N₂ adsorption and dissociation on the surface,
- H blocking of active sites (hydrogen poisoning),
- hydrogenation of NH_x to NH₃, and
- NH₃ desorption (ammonia poisoning),^{3,45}

as illustrated in Figure 5B. Figure 5C distinguishes those elements that prefer a top-layer doping site with a "-I" appendix from those preferring a second-layer doping site indicated with a "-II" appendix, corresponding to a "layer stability" criterion. Additionally, for nonmetal elements we also included a vapor stability criterion, screening out elements that under the chosen reaction conditions would prefer to vaporize as hydrides (e.g., As preferentially evolves as AsH3). With regard to the stability in the presence of oxidizing agents, we recall that Fe-based HB catalysts are rather sensitive to oxygen (or water) poisoning. Indeed, working at less than 10 ppm of O₂ or H₂O is necessary to avoid catalyst degradation in the industrial process. 47 Since most active dopants are more electronegative than iron (e.g.: for silicon 1.90 Pauli electronegativity vs 1.83 for iron), they are expected to be less sensitive than Fe to oxidative poisoning or degradation.

The application of HHTCS to Fe-bcc(111) is displayed in Figure 5C.³ According to the first barrier criterion, only 17 dopant elements led to a barrier lower than the highest barrier of 1.68 eV on the pure Fe surface. Therefore, the other 34 cases (colored yellow in Figure 5C) were not examined further. The second criterion eliminated 7 elements (blue). For the last two criteria, all 7 remaining candidates are better than Fe. Three nonmetal elements were eliminated because of the vapor stability criterion (purple). For the layer-stability criterion, results were as follows.

Cu, Rh, Pd, and Pt favor top-layer doping. Rh and Pt were the best single element dopants for top-layer doping on the Fe(111) surface. The full mechanism for Rh was then examined and found to be the most suitable first-layer dopant, leading to a \approx 3 increase in TOF under Somorjai conditions compared to the undoped Fe-bcc(111) surface.³

Co, Ni, and Si prefer subsurface sites. For subsurface doping, we first considered a pool of 34 transition-metal candidates, and then we extended to 17 nontransition metals (metalloids and main group metals). Only three transition-metal elements (Cr, Co, Ni) prefer second-layer doping sites, but Cr filtered out based on $\rm H_2$ poisoning. Finally, Ni doping was found to be the best, with a predicted 16-fold improvement in the reaction rate. 45

Most nontransition-metal elements preferred first-layer positions or did not improve the primary barrier, but Si was found to both prefer second-layer doping and to improve all the reaction barriers. After full QM/kMC evaluation, we predicted that Si-doped Fe-bcc(111) achieves a 43-fold increase in TOF under Somorjai conditions. Alternatively we predict that Si achieves a TOF similar to HB for pure Fe-bcc(111) but at much less severe conditions; 400 C vs 500 C (HB) and 54 atm vs 200 atm (HB). Thus, we predict Si as the optimal single-dopant.

3.2.2. HHTCS: Application to Fe-bcc(211)R. Having established the mechanism on the Fe-bcc(211)R surface, ² we used HHTCS to test a pool of 49 candidate dopants, including metalloids, main group metals, transition metals, and selected lanthanides. ⁴⁸ Only surface and subsurface doping were considered. Here, we excluded third-layer doping, as the trough region of the reconstructed surface only interacts with troughbonded N atoms which do not participate in the NH₃ synthesis reaction, serving only to lower the surface energy for intermediate states. The full pool of 49 elements along with results of the screening criteria are shown in Figure 6.

From the HHTCS analysis, we found three candidates (Co, Zr, and Ru), all preferring second-layer doping. Co was predicted to have the most beneficial effect on the primary reaction barrier, leading to a reaction mechanism very similar to that on the undoped (211)R surface in Figure 4. We carried out the analysis of the full reaction pathway obtaining, free energies and free energy reaction barriers. These were inputted into the kMC model for the Co-doped Fe-bcc(211)R surface, leading to predicting that Co doping increases the TOF by a factor of 3 with respect to the undoped Fe-bcc(211)R surface under identical conditions. We predict that the Co-doped surface at 40 atm total pressure and T = 773 K achieves the same TOF as the undoped surface at 200 atm total pressure and 773 K. Thus, Co

is suitable as a dopant for an energy-saving process. Next we want to consider ternary doping solutions to further improve the reaction rate on the Fe-bcc(211)R surface.

3.3. Controlling the Shape of Nanoparticles through the Use of Dopants

The QM findings from the Fe-bcc(111), Fe-bcc(110), Fe-bcc(100), and Fe-bcc(211)R surfaces were used to predict nanoparticle shapes via the Wulff construction. ^{29,49} We predict that Fe(100) and Fe-bcc(211)R are more abundant than Fe-bcc(111), as shown in Figure 7A. Clearly, a reshaping more

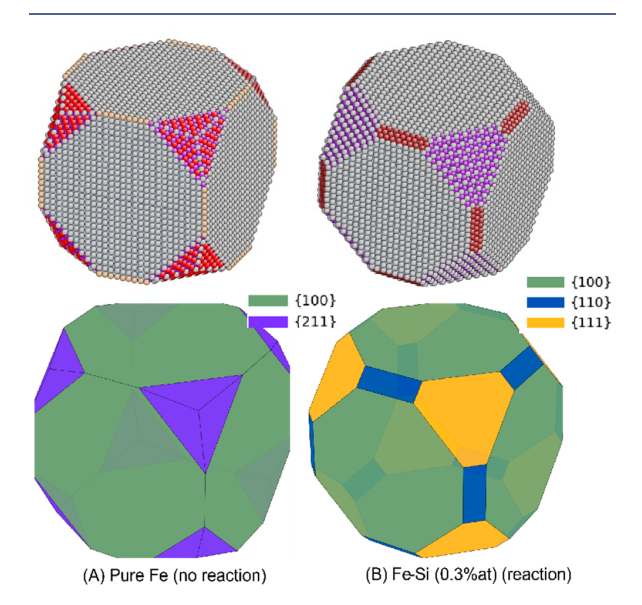


Figure 7. Wulff construction for (A) pure-Fe nanoparticles under noreaction conditions of $P(H_2)=15$ atm, $P(N_2)=5$ atm, T=673 K and (B) optimally Si-doped nanoparticles under reaction conditions of $P(H_2)=15$ atm, $P(N_2)=5$ atm, $P(NH_3)=1$ atom, T=673 K. The atoms in atomistic figures are color coded by coordination number (CN, the CN2, CN4, CN5, CN6, CN7, CN8 are represented by burlywood, gray, red, brown, purple, and light steel blue balls, respectively). In the bottom images blue is (110), gold is (111), green is (100), and purple is (211)R Fe surfaces, respectively. Reproduced from ref 29. Copyright 2021 American Chemical Society.

favorable to Fe-bcc(111) could greatly enhance the catalytic activity of Fe-bcc nanoparticles. Since surface energies depends upon doping, we used a modification of the HHTCS approach to find dopants that optimize this reshaping while also increasing reaction rates.²⁹ We examined 34 candidate dopants and found that 16 of the 34 dopants analyzed can change the nanoparticle shape to increase the surface area of active surface Fe-bcc(111), with 2 of the dopants in particular (Si and Ni) leading to dramatically increased catalytic performance over previous HHTCS studies.^{3,4,45,48}

For Si, we determined a steady-state dynamical Wulff construction to predict the improvement in reaction rate. We found that doping Si into the Fe nanoparticles at an optimal atomic content of $\geq 0.3\%$ leads to rate enhancements by a factor of 56 per nanoparticle under target HB conditions. This in turn leads to a significant reshaping of the nanoparticle structure, as shown in Figure 7B, where the Fe-bcc(111) doped surface becomes more favorable than Fe-bcc(211)R.

4. SPECTROSCOPIC SIGNATURES FOR OPERANDO VALIDATION OF MECHANISTIC FEATURES

One path to validate experimentally the predicted NH₃ synthesis reaction mechanisms on the Fe-bcc catalysts as well as the proposed dopants that improve catalytic efficiency is to correlate the vibrational frequencies of the reaction intermediates predicted by kMC to have significant surface populations with experimental measurements. Thus, we conducted a comprehensive study of the vibrational modes of adsorbed intermediates (N, H, N₂, NH₂, NH₃) in NH₃ synthesis over the most catalytically active Fe-bcc(111) and Fe-bcc(211)R surfaces in both doped and undoped configurations to provide a guide for experimental verification.³⁰

First, we found good agreement between our predictions and available experimental infrared spectroscopy (IR) data collected over the last 30-years for each adsorbed species, $^{50-54}$ validating the accuracy of our predicted IR spectra. 30 In detail, we found H vibrational modes in the range of 1347–1443 cm $^{-1}$, N_2 vibrational modes in the range of 2147–2179 cm $^{-1}$, NH_2 vibrational modes in the range of 1466–1496 cm $^{-1}$, NH_3 vibrational modes in the range of 1092–1161 cm $^{-1}$ across the tested surface configurations and orientations, in good agreement with experimentally determined values.

Next, we analyzed systematically these results to select vibrational modes that differ significantly between doped and undoped systems, or across different facets, or under different experimental conditions, to single out features that could be used experimentally as indicators to monitor doping, faceting, restructuring, and resting-state configurations, with the goal of achieving full validation of the reaction mechanisms. Interestingly, we found and rationalized that

- N₂ species are promising to sample top-layer doping, such as Rh-doping,
- the hindered umbrella mode of adsorbed NH₃ can differentiate surface orientations such as Fe-bcc(111) and Fe-bcc(211)R surfaces (due to the difference in adsorption tilting), in addition to furnishing information on the role of ammonia poisoning on the catalytic rates,
- NH/NH₂ species correlate well with catalyst composition and reaction paths, while
- the perpendicular vibrational mode of adsorbed H adatoms is uniquely sensitive to coadsorbed species and surface coverage, as well as to surface faceting: Febcc(111), Fe-bcc(211), both reconstructed and unreconstructed, and Fe-bcc(110).

We thus suggest IR spectroscopy (both in situ/operando and ex situ) as the characterization tool of choice for experimental mechanistic investigations of the complex reaction mechanisms for ammonia synthesis.³⁰

5. SUMMARY AND PERSPECTIVES

In recent years, computational techniques have been able to predict the complex behavior of surface adsorbates and reaction mechanisms on the facet orientations most catalytically relevant, leading to greatly improved understanding of NH₃ synthesis on Fe catalysts. We reviewed here our recent studies on HB NH₃ synthesis that, for undoped Fe, agree with experimental single crystal studies. We then show a practical hierarchical strategy for in silico optimization of dopants, finding surface selective dopants that can dramatically accelerate NH₃ synthesis. This illustrates our general approach to rational catalyst design of realistically complex, industrially relevant catalytic processes, where

simplified methods such as volcano modeling are ineffective at capturing the dozens reaction steps that can dominate the rates.

First, we derived QM-based reaction FEdiag under realistic reaction conditions and used them in kMC modeling to predict catalytic rates. This led to good agreement with previously reported experimental and theoretical results on reaction rates on Fe-bcc(111) and Fe-bcc(211)R, two of the most important surface orientations. The TOF = 17.7 NH $_3/s$ per 2 × 2 site on Fe-bcc(111) and TOF = 18.7 NH₃/s per 2 \times 2 site on Febcc(211)R under low NH₃ pressure conditions (T = 673 K, P $NH_3 = 1.5 \text{ Torr}$) are consistent with single-crystal experiments. To the best of our knowledge, we have singled out for the first time in our work the importance of hydrogenation (hydrogen migration) barriers in the HB process, and thus the complexity of this industrially relevant catalytic process and the consequent need to go beyond simple volcano modeling to achieve a predictive catalyst rational design. This point is validated by the agreement between predicted and experimental catalytic rates at very low ammonia pressure, under which conditions the N2 dissociation barrier, usually considered as the rate-determining step, becomes less relevant.

To improve catalytic performance on these most active surfaces, we developed a simplified kinetic model which led to a new HHTCS strategy to sift quickly through a large numbers of candidate catalyst modifications by evaluating their effect on key steps along the complex reaction pathway, using a hierarchically ordered set of reaction free-energy barriers. Applying HHTCS to Fe-bcc(111) and Fe-bcc(211)R, we found that subsurface Si doping was most beneficial for Fe-bcc(111), resulting in a predicted 43-fold increase under realistic conditions, with performance equivalent to the undoped surface at similar temperatures (T = 773 K) but at a drastically lower total pressure (P = 20 atm vs P = 200 atm). This makes Si-doped Febcc(111) the most promising for an improved HB process. Similarly, HHTCS predicts that Co subsurface doping on Febcc(211)R can result in a 3-fold increase in reaction rates under standard conditions and up to a 7-fold increase at higher temperatures/pressures.

The predicted surface energies were then used to generate a Wulff construction of Fe nanoparticles to evaluate the extent and contribution of Fe facets to NH3 synthesis. Under no-reaction conditions ($P(H_2, N_2, NH_3) = 15, 5, 0$ atm, T = 673 K), the Febcc(211)R surface plays a significant role. However, with the inclusion of the Si dopant, the nanoparticle shape undergoes significant changes making Si-doped Fe-bcc(111) favorable with Fe-bcc(110) playing a decreased role. This indicates that optimal dopants can appreciably influence the nanoparticle shape and catalyst design.

Finally, to provide a means for experimental validation of the reaction mechanism, we predicted theoretical operando spectroscopic signatures. We found excellent agreement between our predictions and available experimental IR data. Moreover, we found that several surface adsorbates in important configurations (adsorbed N₂, NH_x, and NH₃ species, H adatoms) exhibit spectroscopic signatures that could be used to identify individual configurations on both the doped and undoped Fe-bcc(111) and Fe-bcc(211)R surfaces. This may provide the means for exhaustive validation and reaction monitoring.

To further improve reaction rates on these complex Fe catalysts, we plan to explore the use of multiple dopants (ternary systems) with each targeted to improve performance on a selected surface while accounting for the dopant distribution on

the various facets. Analyzing the role of promoters (such as K or Ba) in conjunction with substitutional dopants is also of interest. More complex cases such as multiple dopants and high-entropy alloys may benefit from the present methods.

Another direction is to pursue increasing the accuracy of computational predictions, e.g., via embedded correlated wave function techniques⁵⁵ or ad hoc corrections as we have explored in ref 3, possibly empowered by machine-learning tools.

ASSOCIATED CONTENT

Supporting Information

The Supporting Information is available free of charge at https://pubs.acs.org/doi/10.1021/acs.accounts.1c00789.

> Schematic depiction of the bcc surface structures here investigated also showing 4-fold binding sites (PDF)

AUTHOR INFORMATION

Corresponding Authors

Qi An – Department of Chemical and Materials Engineering, University of Nevada, Reno, Nevada 89577, United States; orcid.org/0000-0003-4838-6232; Email: qia@unr.edu

Alessandro Fortunelli — Materials and Process Simulation Center (MSC), California Institute of Technology, Pasadena, California 91125, United States; ThC2-Lab, CNR-ICCOM, Consiglio Nazionale delle Ricerche, Pisa 56124, Italy; orcid.org/0000-0001-5337-4450;

Email: alessandro.fortunelli@cnr.it

William A. Goddard, III - Materials and Process Simulation Center (MSC), California Institute of Technology, Pasadena, California 91125, United States; o orcid.org/0000-0003-0097-5716; Email: wag@caltech.edu

Author

Jon Fuller - Department of Chemical and Materials Engineering, University of Nevada, Reno, Nevada 89577, United States

Complete contact information is available at: https://pubs.acs.org/10.1021/acs.accounts.1c00789

The authors declare no competing financial interest.

Biographies

Jon Fuller obtained his BS in Chemistry (with a Physics minor) from Troy University in 2018 and is a PhD student in Materials Science and Engineering (MSE) at UNR. His research interests are the application of QM methods for determining molten salt properties to improve pyroprocessing and molten salt reactor design as well as the computational study of synthesis reactions to influence improved homogeneous and heterogeneous catalyst design.

Qi An obtained his BS in Geophysics from USTC in 2002 and his PhD in Materials Science from Caltech in 2012. He joined the UNR MSE in 2016. His research area is computational materials science covering machine learning, electronic structure calculations and atomistic simulations. His research specifically focuses on heterogeneous catalysis, physical properties of ceramics; computational alloy design; and material behaviors under extreme conditions.

Alessandro Fortunelli obtained his MS in Chemistry (highest honors) from University of Pisa and Scuola Normale in 1983 and his PhD in Theoretical Chemistry from Scuola Normale in March 2012. He joined the Italian National Research Council in March 1984, where he is Research Director at the Institute of Chemistry of OrganoMetallic Compounds (ICCOM). He has developed methods for accelerating computational modeling in molecular and materials sciences, from quantum mechanics to stochastic sampling, and applied these methods to metal nanoclusters/alloys, 2D and nanomaterials, amorphous carbon, and catalysis (homogeneous, heterogeneous, and electrochemical).

William A. Goddard III obtained his BS in Engineering (highest honors) from UCLA in 1960 and his PhD in Engineering Science (with a Physics minor) from Caltech, finishing in Oct. 1964. He joined the Caltech chemistry department in Nov. 1964 where he is now the Charles and Mary Ferkel Professor of Chemistry, Materials Science, and Applied Physics and Director of the Materials and Process Simulation Center. He has been a member of the National Academy of Science since 1984. He has been and continues to be a pioneer in developing methods for QM and reactive molecular dynamics and using these methods for applications to catalysts (homogeneous, heterogeneous, and electrochemical) and nanotechnology.

ACKNOWLEDGMENTS

A.F. gratefully acknowledges the contribution of the International Research Network IRN on Nanoalloys (CNRS). A.F. and W.A.G. received support from NSF (CBET-1805022 and CBET-2005250).

■ REFERENCES

- (1) Qian, J.; An, Q.; Fortunelli, A.; Nielsen, R. J.; Goddard, W. A. Reaction Mechanism and Kinetics for Ammonia Synthesis on the Fe(111) Surface. J. Am. Chem. Soc. 2018, 140, 6288–6297.
- (2) Fuller, J.; Fortunelli, A.; Goddard, W. A., III; An, Q. Reaction Mechanism and Kinetics for Ammonia Synthesis on the Fe(211) Reconstructed Surface. *Phys. Chem. Chem. Phys.* **2019**, 21, 11444–11454
- (3) An, Q.; Shen, Y.; Fortunelli, A.; Goddard, W. A., III QM-Mechanism-Based Hierarchical High-Throughput in Silico Screening Catalyst Design for Ammonia Synthesis. *J. Am. Chem. Soc.* **2018**, *140*, 17702–17710.
- (4) An, Q.; Mcdonald, M.; Fortunelli, A.; Goddard, W. A., III Si-Doped Fe Catalyst for Ammonia Synthesis at Dramatically Decreased Pressures and Temperatures. J. Am. Chem. Soc. 2020, 142, 8223–8232.
- (5) Schlögl, R. Catalytic Synthesis of Ammonia A "Never-Ending Story"? *Angew. Chem., Int. Ed.* **2003**, 42, 2004–2008.
- (6) Ober, J. A.. Mineral Commodity Summaries 2018; U.S. Geological Survey, 2018.
- (7) Mittasch, A.; Frankenburg, W. Early Studies of Multicomponent Catalysts. *Adv. Catal.* **1950**, *2*, 81–104.
- (8) Capdevila-Cortada, M. Electrifying the Haber-Bosch. *Nat. Catal.* **2019**, *2*, 1055.
- (9) Ertl, G. Primary Steps in Catalytic Synthesis of Ammonia. *J. Vac. Sci. & Technol. A* **1983**, *1*, 1247.
- (10) Strongin, D. R.; Somorjai, G. A. The Effects of Potassium on Ammonia Synthesis over Iron Single-Crystal Surfaces. *J. Catal.* **1988**, *109*, 51–60.
- (11) Somorjai, G. A.; Materer, N. Surface Structures in Ammonia Synthesis. *Top. Catal.* **1994**, *1*, 215–231.
- (12) Spencer, N. D.; Schoonmaker, R. C.; Somorjai, G. A. Iron Single Crystals as Ammonia Synthesis Catalysts: Effect of Surface Structure on Catalyst Activity. *J. Catal.* **1982**, *74*, 129–135.
- (13) Strongin, D. R.; Carrazza, J.; Bare, S. R.; Somorjai, G. A. The Importance of C7 Sites and Surface Roughness in the Ammonia Synthesis Reaction over Iron. *J. Catal.* **1987**, *103*, 213–215.
- (14) Hagen, S.; Barfod, R.; Fehrmann, R.; Jacobsen, C.; Teunissen, H. T.; Stahl, K.; Chorkendorff, Ib. New Efficient Catalyst for Ammonia

- Synthesis: Barium-Promoted Cobalt on Carbon. *Chem. Commun.* **2002**, *11*, 1206–1207.
- (15) Kandemir, T.; Schuster, M. E.; Senyshen, A.; Behrens, M.; Schlögl, R. The Haber-Bosch Process Revisited: On the Real Structure and Stability of "Ammonia Iron" under Working Conditions. *Angew. Chem. Int.* **2013**, *52*, 12723–12726.
- (16) Kitchin, J. R. Correlations in Coverage-Dependent Atomic Adsorption Energies on Pd(111). *Phys. Rev. B* **2009**, *79*, 205412.
- (17) Wittreich, G. R.; Liu, S. Z.; Dauenhauer, P. J.; Vlachos, D. G. Catalytic Resonance of Ammonia Synthesis by Simulated Dynamic Ruthenium Crystal Strain. *Sci. Adv.* **2022**, *8*, eabl6576.
- (18) Ertl, G. Reactions at Surfaces: From Atoms to Complexity (Nobel Lecture). *Angew. Chem.* **2008**, 47, 3524–3535.
- (19) Mortensen, J. J.; Hansen, L. B.; Hammer, B.; Nørskov, J. K. Nitrogen Adsorption and Dissociation on Fe(111). *J. Catal.* **1999**, *182*, 479–488
- (20) Zeinalipour-Yazdi, C. D.; Hargreaves, J. S. J.; Laassiri, S.; Catlow, C. R. A. The Integration of Experiment and Computational Modelling in Heterogeneously Catalysed Ammonia Synthesis over Metal Nitrides. *Phys. Chem. Chem. Phys.* **2018**, *20*, 21803—21808.
- (21) Singh, A. R.; Montoya, J. H.; Rohr, B. A.; Tsai, C.; Vojvodic, A.; Nørskov, J. K. Computational Design of Active Site Structures with Improved Transition-State Scaling for Ammonia Synthesis. *ACS Catal.* **2018**, *8*, 4017–4024.
- (22) Hoskuldsson, A. B.; Abghoui, Y.; Gunnarsdottir, A. B.; Skulason, E. Computational Screening of Rutile Oxides for Electrochemical Ammonia Formation. ACS Sustainable Chem. Eng. 2017, 5, 10327—10333
- (23) Wang, Z.; Yu, Z.; Zhao, J. Computational screening of a single transition metal atom supported on the C_2N monolayer for electrochemical synthesis. *Phys. Chem. Chem. Phys.* **2018**, 20, 12835–12844
- (24) Kitano, M.; Kanbara, S.; Inoue, Y.; Kuganathan, N.; Sushko, P. V.; Yokoyama, T.; Hara, M.; Hosono, H. Electride Support Boosts Nitrogen Dissociation over Ruthenium Catalyst and Shifts the Bottleneck in Ammonia Synthesis. *Nat. Commun.* **2015**, *6*, 6731.
- (25) Yiokari, C. G.; Pitselis, G. E.; Polydoros, D. G.; Katsaounis, A. D.; Vayenas, C. G. High-Pressure Electrochemical Promotion of Ammonia Synthesis over an Industrial Iron Catalyst. *J. Phys. Chem. A* **2000**, *104*, 10600–10602.
- (26) Guo, C.; Ran, J.; Vasileff, A.; Qiao, S.-Z. Rational Design of Electrocatalysts and Photo(electro)catalysts for Nitrogen Reduction to Ammonia (NH₃) under Ambient Conditions. *Energy Environ. Sci.* **2018**, *11*, 45–56.
- (27) Liu, H. Ammonia Synthesis Catalyst 100 Years: Practice, Enlightenment and Challenge. *Chin. J. Catal.* **2014**, 35, 1619–1640.
- (28) Wu, T.; Li, P.; Wang, H.; Zhao, R.; Zhou, Q.; Kong, W.; Liu, M.; Zhang, Y.; Sun, X.; Gong, F. Biomass-Derived Oxygen-Doped Hollow Carbon Microtubes for Electrocatalytic N₂-to-NH₃ Fixation under Ambient Conditions. *Chem. Commun.* **2019**, *55*, 2684–2687.
- (29) An, Q.; McDonald, M.; Fortunelli, A.; Goddard, W. A. Controlling the Shapes of Nanoparticles by Dopant-Induced Enhancement of Chemisorption and Catalytic Activity: Application to Fe-Based Ammonia Synthesis. ACS Nano 2021, 15, 1675—1684.
- (30) Fuller, J.; Fortunelli, A.; Goddard, W. A., III; An, Q. Vibrational Spectroscopy Signatures of Catalytically Relevant Configurations for N_2 reduction to NH_3 on Fe Surfaces via Density-Functional Theory. *J. Phys. Chem. C* **2021**, 125, 27919–27930.
- (31) Kresse, G.; Hafner, J. Ab Initio Molecular-Dynamics Simulation of the Liquid-Metal—Amorphous-Semiconductor Transition in Germanium. *Phys. Rev. B: Condens. Matter Mater. Phys.* **1994**, 49, 14251—14269.
- (32) Kresse, G.; Furthmüller, J. Efficiency of Ab-initio Total Energy Calculations for Metals and Semiconductors using a Plane-Wave Basis Set. *Comput. Mater. Sci.* **1996**, *6*, 15–50.
- (33) Kresse, G.; Furthmüller, J. Efficient Iterative Schemes for Ab Initio Total-Energy Calculations using a Plane-Wave Basis Set. *Phys. Rev. B: Condens. Matter Mater. Phys.* **1996**, *54*, 11169–11186.

- (34) Perdew, J. P.; Burke, K.; Ernzerhof, M. Generalized Gradient Approximation Made Simple. Phys. Rev. Lett. 1996, 77, 3865-3868.
- (35) Ernzerhof, M.; Perdew, J. P.; Burke, K. Coupling-Constant Dependence of Atomization Energies. Int. J. Quantum Chem. 1997, 64,
- (36) Johnson, E. R.; Becke, A. D. A Post-Hartree-Fock Model of Intermolecular Interactions: Inclusion of Higher-order Corrections. J. Chem. Phys. 2006, 124, 174104.
- (37) Henkelman, G.; Uberuaga, B. P.; Jonsson, H. A climbing image nudged elastic band method for finding saddle points and minimum energy paths. J. Chem. Phys. 2000, 113, 9901-9904.
- (38) Lin, R.-J.; Li, F.-Y.; Chen, H.-L. Computational Investigation on Adsorption and Dissociation of the NH3 Molecule on the Fe(111) Surface. J. Phys. Chem. C 2011, 115, 521-528.
- (39) Hidaka, H.; Watanabe, M.; Kouchi, A.; Watanabe, N. FTIR Study of Ammonia Formation via the Successive Hydrogenation of N Atoms Trapped in a Solid N2Matrix at Low Temperatures. Phys. Chem. Chem. Phys. 2011, 13, 15798-15802.
- (40) Baxter, R. J.; Hu, P. Insight into Why the Langmuir-Hinshelwood Mechanism is Generally Preferred. J. Chem. Phys. 2002, 116, 4379-
- (41) Hassold, E.; Löffler, U.; Schmiedl, R.; Grund, M.; Hammer, L.; Heinz, K.; Müller, K. Hydrogen Induced Missing Row Reconstruction of Fe (211). Surf. Sci. 1995, 326, 93-100.
- (42) Schmiedl, R.; Nichtl-Pecher, W.; Heinz, K.; Müller, K.; Christmann, K. Hydrogen on Fe(211): Commensurate and Reconstructed Phases. Surf. Sci. 1990, 235, 186-196.
- (43) McKay, H.; Jenkins, S.; Wales, D. Theory of NHx ± H Reactions on Fe{211}. J. Phys. Chem. C 2009, 113, 15274-15287.
- (44) Gillespie, D. T. A General Method for Numerically Simulating the Stochastic Time Evolution of Coupled Chemical Reactions. J. Comput. Phys. 1976, 22, 403-434.
- (45) Mcdonald, M.; Fuller, J.; Fortunelli, A.; Goddard, W. A., III; An, Q. Highly Efficient Ni-Doped Iron Catalyst for Ammonia Synthesis from Quantum-Mechanics-Based Hierarchical High-Throughput Catalyst Screening. J. Phys. Chem. C 2019, 123, 17375-17383.
- (46) Nørskov, J. K.; Bligaard, T.; Rossmeisl, J.; Christensen, C. H. Towards the computational design of solid catalysts. Nat. Chem. 2009, 1. 37-46.
- (47) Lui, H. Ammonia Synthesis Catalysts: Innovation and Practice; World Scientific, 2013.
- (48) Fuller, J.; Fortunelli, A.; Goddard, W. A., III; An, Q. Discovery of Dramatically Improved Ammonia Synthesis Catalysts through Hierarchical High-Throughput Catalyst Screening of the Fe(211) Surface. Chem. Mater. 2020, 32, 9914-9924.
- (49) Wulff, G. On the Question of Speed of Growth and Dissolution of Crystal. Surfaces. Z. Krystallogr. 1901, 34, 449-530.
- (50) Tsai, M.-C.; Ship, U.; Bassignana, I. C.; Kuppers, J.; Ertl, G. A Vibrational Spectroscopy Study on the Interaction of N2 with Clean and K-Promoted Fe(111) Surfaces: π -Bonded Dinitrogen as Precursor for Dissociation. Sur. Sci. 1985, 155, 387-399.
- (51) Grunze, M.; Golze, M.; Hirschwald, W.; Freund, H.-J.; Pulm, H.; Seip, U.; Tsai, M.-C.; Ertl, G.; Kuppers, J. pi-Bonded N₂ on Fe(111): The Precursor for Dissociation. Phys. Rev. Lett. 1984, 53, 850-853.
- (52) Erley, W.; Ibach, H. Vibrational Spectra of Ammonia Adsorbed on Fe(110). Surf. Sci. 1982, 119, L357-L362.
- (53) Erley, W.; Ibach, H. The Adsorption of Ammonia on an Fe(110) Single-Crystal Surface Studied by High-Resolution Electron Energy-Loss Spectroscopy (EELS). J. Electron Spectrosc. Relat. Phenom. 1983, 31, 161-174.
- (54) Novell-Leruth, G.; Valcarcel, A.; Clotet, A.; Ricart, J. M.; Perez-Ramirez, J. DFT Characterization of Adsorbed NHx species on Pt(100) and Pt(111) Surfaces. J. Phys. Chem. B 2005, 109, 18061-18069.
- (55) Libisch, F.; Huang, C.; Carter, E. A. Embedded Correlated Wavefunction Schemes: Theory and Applications. Acc. Chem. Res. 2014, 47, 2768-2775.
- (56) Bartok, A. P.; Gillan, M. J.; Manby, F. R.; Csanyi, G. Machine-Learning Approach for One- and Two-Body Corrections to Density

Functional Theory: Applications to Molecular and Condensed Water. Phys. Rev. B 2013, 88, 054104.

☐ Recommended by ACS

Cost and Performance Targets for Fully Electrochemical **Ammonia Production under Flexible Operation**

Nikifar Lazouski, Dharik S. Mallapragada, et al.

JULY 19, 2022

ACS ENERGY LETTERS

READ C

Dynamic Control of Liquid Biomass Digestate Distillation Combined with an Integrated Solar Concentrator Cycle for **Sustainable Nitrogen Fertilizer Production**

Joshua C. Centorcelli, Jonas Baltrusaitis, et al.

MAY 25, 2022

ACS SUSTAINABLE CHEMISTRY & ENGINEERING

READ **'**

Spatial Variation in Cost of Electricity-Driven Continuous **Ammonia Production in the United States**

Abhishek Bose, Dharik S. Mallapragada, et al.

JUNE 08, 2022

ACS SUSTAINABLE CHEMISTRY & ENGINEERING

READ **'**

Gaseous CO, Coupling with N-Containing Intermediates for Key C-N Bond Formation during Urea Production from Coelectrolysis over Cu

Guo-Lin Yang, Mu-Jeng Cheng, et al.

SEPTEMBER 06, 2022

ACS CATALYSIS

READ

Get More Suggestions >